Journal of Aerosol Science 51 (2012) 57–65

Contents lists available at SciVerse ScienceDirect

Journal of Aerosol Science

journal homepage: www.elsevier.com/locate/jaerosci

From electrostatic precipitation to nanoparticle generation

Chih-Wei Lin [a], Sheng-Hsiu Huang [a], Yu-Mei Kuo [b], Kuang-Nan Chang [a], Chong-Sin Wu [c], Chih-Chieh Chen [a,*]

[a] Institute of Occupational Medicine and Industrial Hygiene, National Taiwan University, 17 Xu-Zhou Road, Taipei 10055, Taiwan
[b] Department of Occupational Safety and Health, Chung Hwa University of Medical Technology, Taiwan
[c] Department of Mechanical Engineering, National Chiao Tung University, Taiwan

ARTICLE INFO

Article history:
Received 29 March 2011
Received in revised form
4 March 2012
Accepted 23 March 2012
Available online 7 April 2012

Keywords:
Electrostatic precipitator
Nanoparticle
Corona discharge
Filtration

ABSTRACT

This work demonstrated that an electrostatic precipitator (ESP), originally designed for dust collection, could become a nanoparticle generator under specific operating conditions. A lab-scale wire-plate positive ESP was built for measuring aerosol penetration and generation rate. The carrier air was filtered by activated charcoal, silica gel and HEPA filters to remove potential contaminants. The data, obtained in both power-on and power-off modes, were utilized to calculate penetration and generation rate of aerosol.

The results showed that air temperature appeared to have a strong effect on ESP nanoparticle generation. At temperature above 37 °C and flow rate below 9 L/min, the nanoparticle penetration of ESP exceeded 100%, indicating that the ESP was generating aerosol particles. Sputtering on the corona discharger appeared to be the key mechanism of aerosol generation. The ozone concentration increased with increasing corona current. The ESP reached a maximum number concentration at the electric field strength of 4.8 kV/cm when the air flow and temperature were fixed at 6 L/min and 40 °C, respectively. The particle size ranged from 5 to 40 nm, with a mode around 12 nm. Elementary components of the discharge wire were detected on the filter samples collected downstream the ESP and ground plates, indicating that nanoparticles were generated from the discharge wire.

© 2012 Elsevier Ltd. All rights reserved.

1. Introduction

Aerosol exposure has been linked to cardiopulmonary diseases, children lung function loss and asthma (Koenig et al., 1993; Gehring et al., 2006; Weichenthal et al., 2007). In semiconductor industry, particles deposited on wafers could reduce yield and increase cost (Cooper, 1986; Pui et al., 1990). The way to reduce health effects and industrial loss is to decrease particle concentration to the lowest possible. Electrostatic precipitators (ESPs) are devices commonly used to remove charged particles in gas by electrostatic force. It is characterized by high collection efficiency, low pressure drop and low maintenance requirements (Mizuno, 2000).

Steps in Particle collection in an ESP involve generating unipolar ions, charging particles, and collecting charged particles by the electric field. Normally, an ESP can be divided into the corona discharge region and the collection region. The corona discharger is a unipolar ion generator that can generate positive or negative ions. It comprises the discharge electrode and the grounded electrode. The discharge electrode can be needles or wires of different shapes. The asymmetric

* Corresponding author. Tel.: +886 2 33668086; fax: +886 2 23938631.
E-mail address: ccchen@ntu.edu.tw (C.-C. Chen).

0021-8502/$ - see front matter © 2012 Elsevier Ltd. All rights reserved.
http://dx.doi.org/10.1016/j.jaerosci.2012.03.005

shape of the electrode contributes to generate a high non-uniform electric field. In the corona discharge region, ions are accelerated to ionize other air molecules, thus causing the phenomenon known as electron avalanche. Particles flowing through the corona discharge region could carry high charges by diffusion charging and field charging. Charged particles then move toward collection plates following the field lines.

ESPs are commonly employed to capture particles with high efficiency. However, it also has drawbacks, such as ozone production and particle generation. Ozone is harmful to health and damaging to materials. Yet, ozone concentration can be suppressed by varying wire material, changing discharge polarity, and decreasing applied current (Boelter and Davidson, 1997; Yehia and Mizuno, 2005). Generation of particles from the corona discharger has been reported in several studies. Nevertheless, this phenomenon was not observed in every corona discharger, probably due to the difference in dimensions of corona discharger and the operating conditions.

In an industrial ionizer, particles could only be detected in the region at 60 cm from the discharge wire, and the particle size ranged from several nm to 1 μm (Liu et al., 1987). Why particles could not be detected at greater distance from the discharge wire remains unknown. It is likely that particles generated from the discharge wire are captured by the ionizer itself due to electric field. Stommel and Riebel (2004) also discovered particle generation from the corona discharger, but the particles disappeared after the strength of radioactive sources was enhanced. Moreover, because the diameter of particles generated from the corona discharger was smaller than 100 nm, the particle counting efficiency of aerosol instruments may be part of the reason why not every researcher observed this phenomenon (Romay et al., 1994).

The principal mechanism for particle generation of ESP was found to be the sputtering of metal electrode (Romay et al., 1994). In a corona discharger, ions could acquire energy in a strong electric field and move toward the discharge wire. When ions have enough energy to break the atomic bond, the nanoparticles were knocked out due to these collisions. The ion energy acquired by ions is mainly determined by the electric field strength. Increasing applied voltage can generate larger particles because ions gain higher energy to knock more particles out (Biris et al., 2004). The distance between electrodes did not change particle generation (Romay et al., 1994). By careful control of the tip shape, particle generation could be suppressed (Hobbs et al., 1990). The material of discharge wire played an important role in particle generation. Using tungsten or molybdenum to replace silicon or stainless steel as electrode could decrease particle generation because molybdenum and tungsten are harder (Romay et al., 1994).

Overall, particle generation from corona discharger is confirmed, but the mechanism has not been systematically investigated. Therefore, the objective of the present study was to characterize the transition of an ESP from a dust collector to a nanoparticle generator.

2. Experimental materials and methods

In order to conduct the experiment of aerosol penetration through an ESP, a lab-scale wire-plate ESP and the test system were built, as shown in Fig. 1. The test chamber, 6 cm in height and 10 cm in width, was made of acrylic. The discharge electrode was made of stainless steel (grade 304), with a diameter of 0.1 mm and placed in the middle of the ESP. The collection plates were made of aluminum with a width of 2 mm and a length of 6 cm. The distance between two collection plates was 1 cm. The wire-to-plate distance was 0.5 cm.

The carrier air was filtered by activated charcoal, silica gel and HEPA filters, in order to avoid the influence of humidity, organic vapor and aerosol particles. The humidity was found to be less than 10% RH. The heater with feedback control was employed to maintain a stable air temperature. Air temperatures, upstream and downstream the ESP, were measured using two k-type thermocouples. The first thermal couple was installed upstream of the ESP to monitor and provide feedback to the heater, as well as to maintain a stable temperature with a standard deviation of less than 0.08 °C.

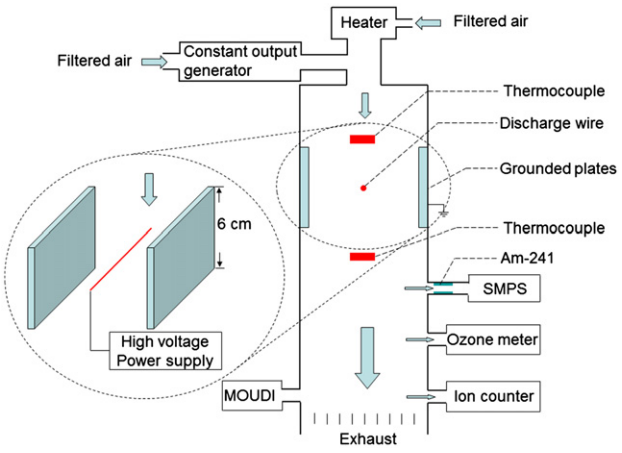

Fig. 1. Schematic diagram of experimental setup.

The temperature was varied from 31 to 43 °C to study the temperature dependency. Another thermal couple was installed downstream the ESP to monitor the temperatures in 'ON' and 'OFF' modes. The temperature of the ESP in the 'ON' mode was higher than that in the 'OFF' mode because of the electrical energy added into the test system. The distance between these two thermal couples was 10 cm, as shown in Fig. 1. The test chamber was made of transparent acrylic for easy observation of electrode sputtering. A direct current power supply (model Sl50PN300, Spellman High Voltage Electronics Corporation, Plainview, NY) was employed to energize the corona discharger. This power supply, which needed to be grounded for proper functioning, was equipped to monitor and display the current output to the ESP.

For aerosol penetration tests, a constant output atomizer (model 3076, TSI Inc., St. Paul, MN) was employed to generate challenging potassium sodium tartrate (PST) aerosols. The total flow rate through the ESP was the sum of flows through the aerosol generator and the heater. The flow rate of constant output aerosol generator was fixed at 1.3 L/min. Aerosol output from TSI model 3076 (as a conventional recirculating atomizer), when used for a long period of time, might show slight difference in number concentration and size distribution because of water evaporation. However, for aerosol penetration tests, the sampling time was only 5 min, and the effect of water evaporation was negligible. A condensation particle counter (CPC, model 3022, TSI Inc.) was employed to check and ensure aerosol uniformity in the test section of the ESP. The lower detection limit of CPC 3022 is about 7 nm (50% efficiency).

A scanning mobility particle sizer (SMPS, model 3934U, TSI Inc.) was employed to measure the aerosol concentration and size distribution for particles smaller than 200 nm. The default flow rate of SMPS was 0.3 L/min. Data on particle number concentration and size distribution were obtained in both power-on and power-off modes. There data were utilized to characterize the nanoparticles generated from the ESP. A radioactive source, 10 mCi Am-241, was employed to neutralize particles before aerosol output was sampled into the SMPS. A Nano-MOUDI (model 115, MSP Inc.) was employed to collect particles generated from ESP. The filtered samples of generated particles were analyzed using scanning electron microscopy, transmission electron microscopy and energy disperse X-ray. The TEM copper screen filter (100 mesh) was placed downstream the ESP and sampled for 8 h. The primary filtration mechanism was diffusion since the ESP-generated particles were smaller than 100 nm. The ozone and ion concentrations were monitored by an ozone analyzer (model 49–100/103, Philips, Olathe, KS) and an ion counter (AlphaLab, West Salt Lake City, UT), respectively. The sampling flow of the ozone analyzer was 1 L/min. The sampling locations of SMPS and ozone analyzer were 20 and 15 cm downstream the ESP, respectively.

3. Results and discussion

The effect of air velocity on the characteristics of current–voltage curve is shown in Fig. 2. The corona discharge onset voltage was 3.8 kV. As can be seen, the *I–V* curve apparently shifted to the right with increase in velocity, indicating that some of the ions escaped from the collection region. For example, at applied voltage of 6 kV, when velocity increased from 0 to 150 cm/s, the electrometer readings decreased from 420 to 370 μA, a 12% reduction. As reported in a previous study (Zhuang et al., 2000), such reudction was due to some of the ions not having enough time to reach the grounded plate as velocity increased. In addition, the number of localized discharge spots on the discharge wire could be affected by the air flow, leading to changes in the corona current (Yehia et al., 2000).

Aerosol penetration is a useful index for evaluating ESP performance. Fig. 3 shows aerosol penetration through the ESP as a function of particle size under five different temperatures ranging from 31 to 43 °C, when air flow was fixed at 9 L/min (equivalent to velocity of 10 cm/s). The GSDs of particle distribution were 1.79 and 1.78 before and after the experiment, respectively. For particles larger than 30 nm, aerosol penetration increased with increasing aerosol size. Notice that aerosol penetration remaining the same with changes in temperature indicates that temperature difference in this range did not

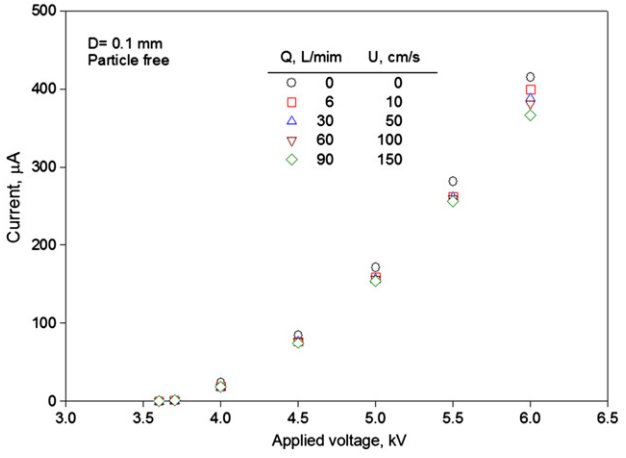

Fig. 2. *I–V* curve under different flow rate.

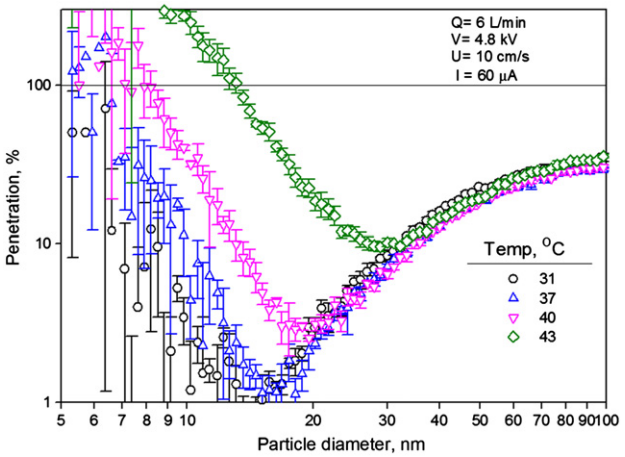

Fig. 3. ESP penetration as a function of particle size under different temperature.

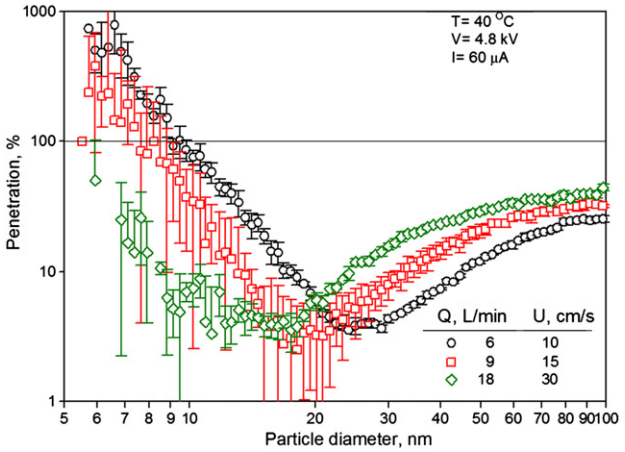

Fig. 4. ESP penetration as a function of flow rate.

significantly affect the particle charging efficiency, aerosol electrical mobility, and field strength. Therefore, aerosol collection efficiency remained unchanged. However, for particles smaller than 20 nm, aerosol penetration increased with increasing air temperature. It has been reported that aerosol penetration in the nanoparticle region was attributed to the partial charging effect (Huang and Chen, 2002). However, aerosol penetration should not exceed 100% even if all particles were not charged. For temperature higher than 37 °C, the nanoparticle penetration exceeded 100%, indicating that at least some of the nanoparticles were generated by the ESP. It is speculated the particles were knocked out from the oxidation layer of discharge wire surface. In an ESP, a positive corona had higher oxidation rate than a negative corona because negative oxygen ions would be attracted by the positive discharge wire (Yehia and Mizuno, 2005). It has been reported that oxidation rate constant of stainless steel increased with increasing temperature (Wild, 1977). Hence, particle penetration exceeded 100% and increased with increasing temperature. In our current experimental setup, we could not measure the temperature surrounding the SS wire using a thermocouple because the plasma density near the wire was too strong. Nevertheless, the surface temperature of the corona wire under similar conditions has been reported to be around 800 K in a corona discharge (Ono et al., 2010), which explained the probable oxidation of SS wire in the present study. The air temperature was recorded at the location of 5 cm downstream the corona discharge wire. The downstream air temperature was 0.5 to 1 °C higher than the upstream temperature, depending on the amount of electrical energy added to the experimental system. The air temperature was much lower than the SS wire temperature because gas temperature decreased rapidly with increasing distance away from the discharge electrode (Ono et al., 2010).

The effect of flow rate (ranging from 6 to 18 L/min) on aerosol generation (<20 nm) and aerosol penetration (>20 nm) is shown in Fig. 4. For particles larger than 20 nm, particle penetration increased with increasing flow rate because of shorter particle retention time in the ESP. For nanoparticles, the penetration (or the nanoparticle generation) increased with decreasing flow rate. Aerosol penetration exceeded 100% when the flow rate was lower than 9 L/min. This flow dependency indicated that the heat generated by the corona discharger was probably carried away by the air flow. Hence, the oxidation rate, and, therefore, the nanoparticle generation rate decreased with increasing flow rate.

It has been reported that secondary organic aerosol could be produced by the reaction between ozone and organic vapors in an ESP (Waring et al., 2008). In order to confirm that the particles were generated directly from the ESP, the dilution carrier air was filtered by a HEPA filter and an activated charcoal bed to remove both aerosol particles and organic vapor. To demonstrate the stability of ESP nanoparticle generation, the challenge aerosol generator was turned off. The ESP nanoparticle generation rate with time is shown in Fig. 5. Particles were detected by the particle counter as soon as the ESP corona discharger was turned on, when the flow rate was 6 L/min and the current was 30 μA. Particle concentration increased sharply at the beginning, and then decreased to a stable level. The sharp increase in aerosol concentration signaled the beginning of aerosol generation while the slow decrease in aerosol concentration with operating time could not be thoroughly explained at this time. We speculated that the oxidized layer on the wire surface was bombarded by the ions and the layer became thinner when the particles were knocked out. Hence, particle concentration decreased with operating time. When the ESP was turned off, particle concentration sharply increased again and then reduced to zero. Such marked up-and-down pattern was attributed to the disappearance of electric field as soon as the ESP was turned off and the residual particles penetrated through the ESP and were detected by the CPC. This phenomenon also indicated that nanoparticles generated by ESP could be captured by the ESP itself, depending on the operating conditions.

The ESP-generated particle concentration was a function of electric field strength, as shown in Fig. 6. Particle concentration reached a maximum when the electric field was around 4.8 kV/cm, with flow rate and temperature fixed at 6 L/min and 40 °C, respectively. The inference was that ions could only obtain less energy when the electric field strength was lower than 4.8 kV/cm. Hence, particle concentration decreased with decreasing electric field strength. Although ions could get higher energy when the electric field strength exceeded 4.8 kV/cm, the ESP collected particles more efficiently, thus resulting in lower aerosol concentration. Such finding indicated that once the corona discharge was turned on, ESP particle generation was activated, even though the current and electric field strength were low.

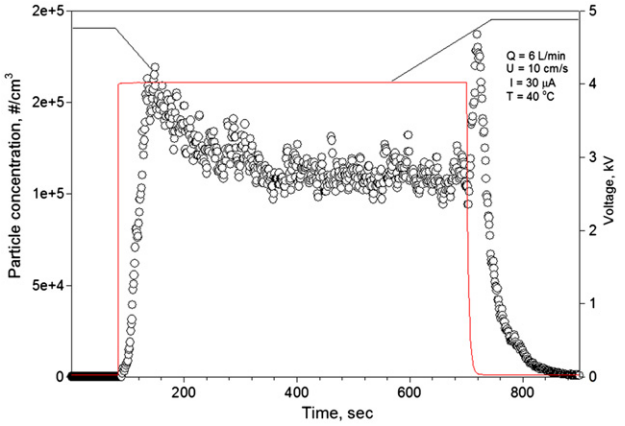

Fig. 5. ESP generates particles when corona discharge was activated.

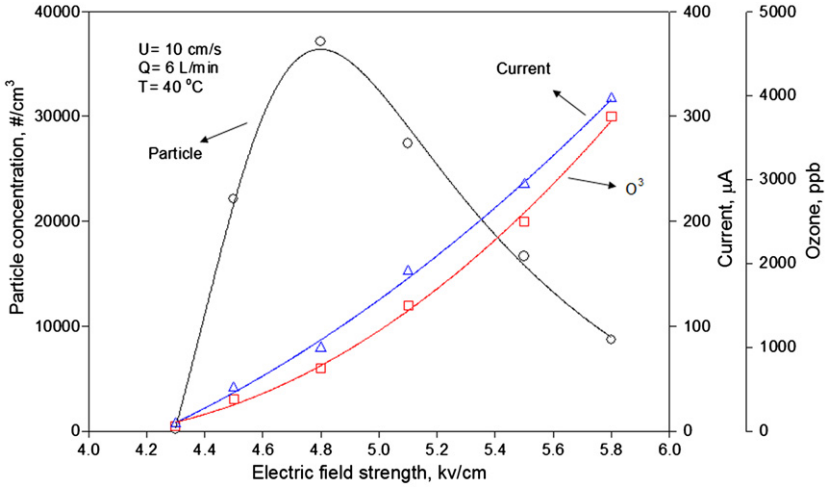

Fig. 6. Particle concentration as a function of electric field strength.

Particle generation from corona dischargers has been reported, but the dimensions of corona discharger and the operating conditions in these studies were all different. This partially explained why aerosol generation by corona dischargers was not found in too many studies. Particle generation might be reduced by decreasing applied voltage (Romay et al., 1994). A dual jet design also reduced the particle generation from an air ionizer (Takeuchi et al., 2003). In this work, it has been confirmed that the particle generation by ESP could be affected by air velocity, temperature and electric field strength. We speculate that ESP generates particles near the corona discharge electrode as soon as corona discharge is turned on. The key for an ESP to become a particle generator is the ESP collection efficiency. An ESP would not become an "apparent" particle generator if the aerosol penetration through this ESP is less than 100%, although the ESP might already be generating particles.

The ozone concentration correlated quite well with the corona current, as shown by the two nearly parallel curves in Fig. 6. This tendency was in good agreement with the finding of Huang and Chen (2001). The ozone production rate was in line with previous studies (Boelter and Davidson, 1997; Chen and Davidson, 2002), as shown in Fig. 7, where the ozone production rate was shown as a function of linear current density. The discharge wire was 0.1 mm in diameter. The ozone production rate increased with increasing current density because of the increase in electron density.

To demonstrate long-term stability, particle generation of the ESP was activated and monitored, eight hours a day for up to seven days. Fig. 8 shows that particle concentration increased with operating time. The mode of particle size ranged from 10 to 20 nm, which was in a good agreement with the results obtained by Romay et al. (1994) and Liu et al. (1987). The increasing trend of aerosol concentration was probably because the oxidized layer became thicker with time. It was also hypothesized that the rough surface (to be shown below in Fig. 9) contributed to form higher electric field on the discharge wire surface and enhance the ion energy because corona discharge tends to occur between two asymmetrical points. The more asymmetrical the structure of the corona discharger is, the higher the electric field strength near the discharge wire will be. The electric field strength as a function of surface roughness and the electric field strength on the microscopic regions of the discharge electrode have been reported to be larger than the average electric field strength

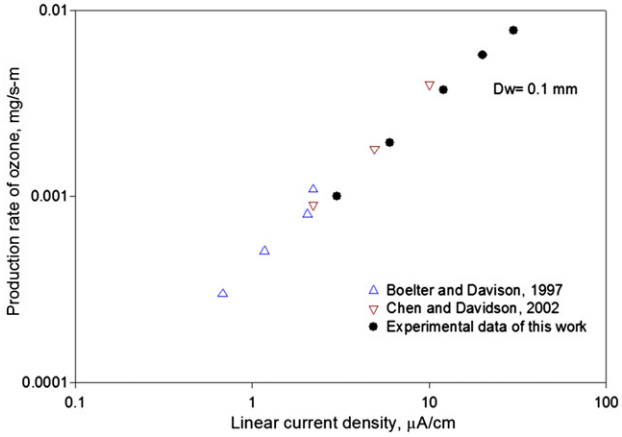

Fig. 7. Comparison of ozone production rate at different current density.

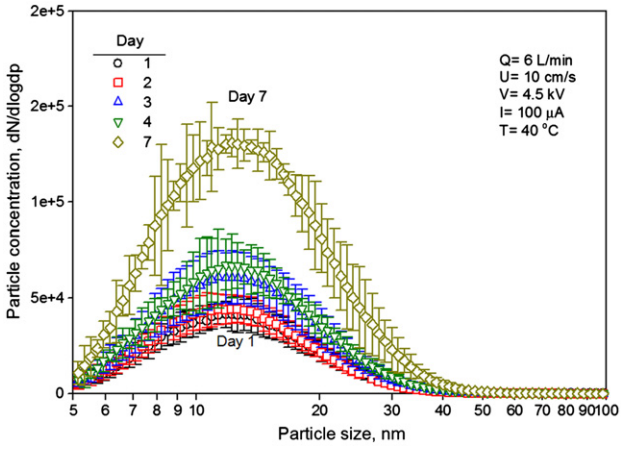

Fig. 8. Particle number concentration increased with operating time.

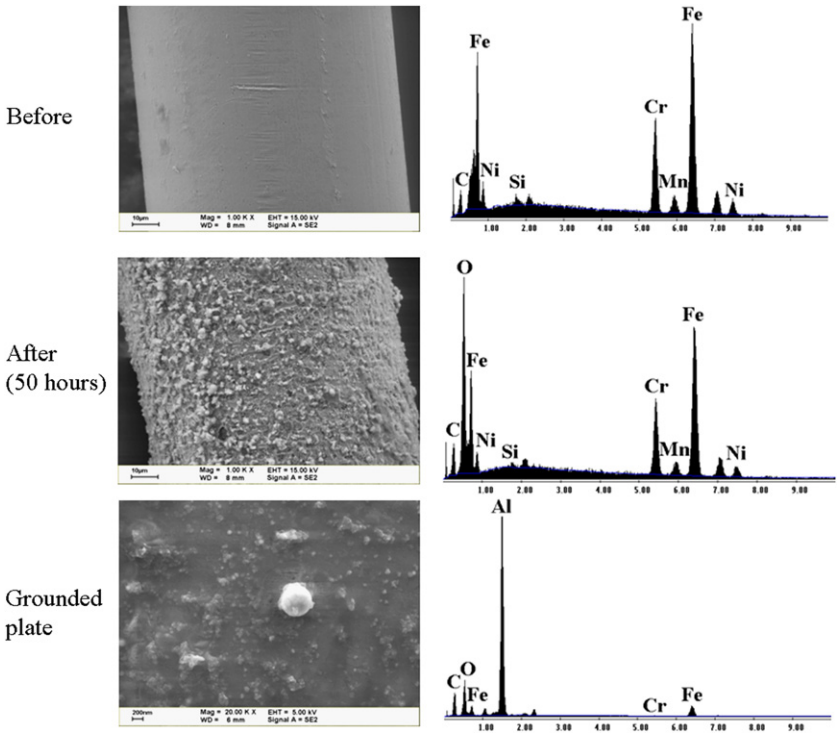

Fig. 9. SEM images and EDX data of nanoparticles generated from corona discharge.

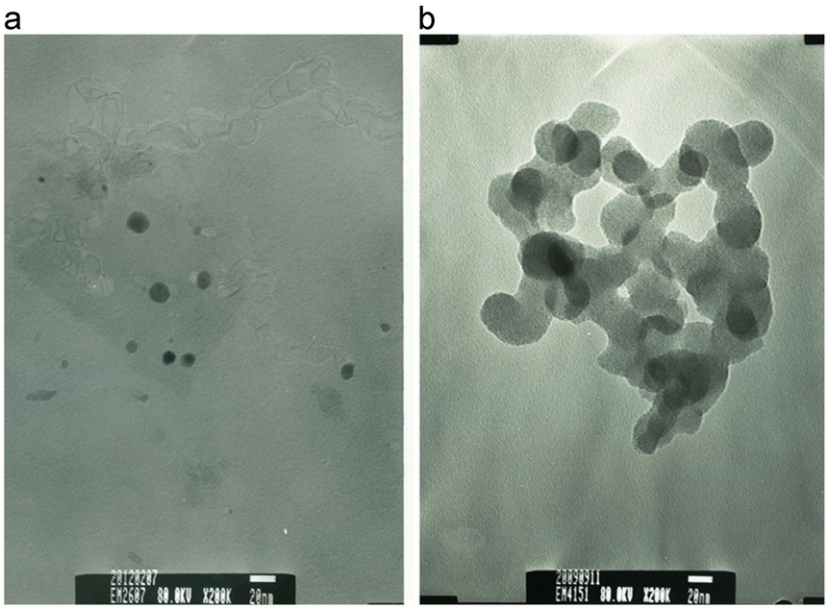

Fig. 10. TEM image of nanoparticles generated from corona discharge. (a) Primary size and (b) Agglomerate.

(Lazi and Persson, 2010; Mahdy et al., 1998). Comparing pictures of the discharge wire before and after use shows many small holes on the discharge wire surface after use. The change of surface condition might result in higher electric field strength near the holes. It is worthwhile to mention that, after use, a brown layer formed on the surface of discharge wire and erosion could be observed from the SEM photos.

The SEM photos and EDX patterns of discharge wires before and after use were shown in Fig. 9. Before use, the surface of corona discharge wire was smooth, and EDX data showed that iron, chromium, and cobalt were its main components. After use, the surface of corona discharge wire became rough. The collisions between ions and wire surface resulted in

small holes on the discharge wire. The oxygen measured by EDX indicated that oxide was formed on the discharge wire. Both chromium and iron were also detected on the MOUDI filter because some of the ESP-generated particles were collected. The particle image analyzed by TEM was shown in Fig. 10. Chemical composition analysis was not performed because the samples were collected on the TEM grid. However, the major components of the SS wire, namely Cr and Fe, detected on the MOUDI filter provided solid evidence that the ESP-generated nanoparticles were originated from the SS electrode. The size of ESP-generated particles ranged from 5 to 40 nm, according to the SMPS data shown in Fig. 8. The TEM image shown in Fig. 10(a) demonstrates that the primary size of particles generated from ESP was about 5 to 20 nm, coincidental with the SMPS measurements. However, larger particles could also be found in the form of aggregate, as shown in Fig. 10(b).

4. Conclusions

This study confirmed that an ESP could also be a nanoparticle generator. For the ESP tested in the present study, its performance remained unchanged for particles larger than 40 nm. However, for particles smaller than 20 nm, aerosol penetration could reach 100%, indicating that the ESP was generating nanoparticles. Sputtering on the corona discharger appeared to be the principal mechanism of aerosol generation. The air temperature had a strong effect on ESP nanoparticle generation, but the mechanisms need to be studied further.

In this work, the wire-plate ESP became a particle generator when the air velocity was below 9 L/min (15 cm/s), the temperature was higher than 37 °C, and the electric field strength was 4.8 kV/cm. There seemed to be a point of operation for the most efficient ESP aerosol generation, which is likely dependent on the electric field strength, air flow and air temperature. For the ESP tested, the maximum concentration occurred at electric field strength of 4.8 kV/cm, flow rate of 6 L/min, and temperature of 40 °C. The particle size ranged from 5 to 40 nm, with a mode around 12 nm. The ozone concentration increased with increasing current. The correlation was almost perfect. After use, the discharge wire surface was covered with a layer of oxidized material.

The oxidized materials accumulated on the surface of discharge wire appeared to influence the aerosol generation rate. For continuous operation, the aerosol generation rate decreased slowly as the layer became thinner. However, the oxidized layer became thicker if the wire was left to be exposed to air for days (Chen and Davidson, 2002).

Acknowledgments

This study was supported by the National Science Council of Taiwan (Grant No. NSC99-2221-E-002-069-MY3). The authors would like to thank Chia-Ying Chien of Instrumentation Center, National Taiwan University for Transmission Electron Microscope experiments.

References

Biris, A.S., De, S., Mazumder, M.K., Sims, R.A., Buzatu, D.A., & Mehta, R. (2004). Corona generation and deposition of metal nanoparticles on conductive surfaces and their effects on the substrate surface texture and chemistry. *Particulate Science and Technology*, *22*, 405–416.

Boelter, K.J., & Davidson, J.H. (1997). Ozone generation by indoor, electrostatic air cleaners. *Aerosol Science and Technology*, *27*, 689–708.

Chen, J., & Davidson, J.H. (2002). Ozone production in the positive DC corona discharge: model and comparison to experiments. *Plasma Chemistry and Plasma Processing*, *22*(4), 495–522.

Cooper, D.W. (1986). Particulate contamination and microelectronics manufacturing: an introduction. *Aerosol Science and Technology*, *5*, 287–299.

Gehring, U., Heinrich, J., Kramer, U., Grote, V., Hochadel, M., Sugiri, D., Kraft, M., Rauchfuss, K., Eberwein, H.G., & Wichmann, H.E. (2006). Long-term exposure to ambient air pollution and cardiopulmonary mortality in women. *Epidemiology*, *17*, 545–551.

Hobbs, P.C.D., Gross, V.P., & Murray, K.D. (1990). Suppression of particle generation in a modified clean room corona air ionizer. *Journal of Aerosol Science*, *21*, 463–465.

Huang, S.H., & Chen, C.C. (2001). Filtration characteristics of a miniature electrostatic precipitator. *Aerosol Science and Technology*, *35*, 792–804.

Huang, S.H., & Chen, C.C. (2002). Ultrafine aerosol penetration through electrostatic precipitators. *Environmental Science and Technology*, *36*, 4625–4632.

Koenig, J.Q., Larson, T.V., Hanley, Q.S., Rebolledo, V., Dumler, K., Checkoway, H., Wang, S.Z., Lin, D.Y., & Pierson, W.E. (1993). Pulmonary function changes in children associated with fine particulate matter. *Environmental Research*, *63*, 26–38.

Lazi, P., & Persson, B.N.J. (2010). Surface-roughness-induced electric-field enhancement and triboluminescence. *EPL (Europhysics Letters)*, *91*(4), 46003.

Liu, B.Y.H., Pui, D.Y.H., Kinstley, W.O., & W, G. (1987). Aerosol charging and neutralization and electrostatic discharge in clean rooms. *Journal of Environmental Sciences*, *30*, 5.

Mahdy, A.M., Anis, H.I., & Ward, S.A. (1998). Electrode roughness effects on the breakdown of air-insulated apparatus. *IEEE Transactions on Dielectrics and Electrical Insulation*, *5*(4), 612–617.

Mizuno, A. (2000). Electrostatic precipitation. *IEEE Transactions on Dielectrics and Electrical Insulation*, *7*, 615–624.

Ono, R., Teramoto, Y., & Oda, T. (2010). Effect of humidity on gas temperature in the afterglow of pulsed positive corona discharge. *Plasma Sources Science and Technology*, *19*, 015009.

Pui, D.Y.H., Ye, Y., & Liu, B.Y.H. (1990). Experimental study of particle deposition on semiconductor wafers. *Aerosol Science and Technology*, *12*, 795–804.

Romay, F.J., Liu, B.Y.H., & Pui, D.Y.H. (1994). A sonic jet corona ionizer for electrostatic discharge and aerosol neutralization. *Aerosol Science and Technology*, *20*, 31–41.

Stommel, Y.G., & Riebel, U. (2004). A new corona discharge-based aerosol charger for submicron particles with low initial charge. *Journal of Aerosol Science*, *35*(9), 1051–1069.

Takeuchi, M., Imazono, H., Terashige, T., Kusakari, S., Tsuruta, N. & Okano, K., 2003. Contamination control of a corona discharge air ionizer, Semiconductor Manufacturing, 2003 IEEE International Symposium on, pp. 483–486.

Waring, M.S., Siegel, J.A., & Corsi, R.L. (2008). Ultrafine particle removal and generation by portable air cleaners. *Atmospheric Environment*, *42*, 5003–5014.

Weichenthal, S., Dufresne, A., & Infante-Rivard, C. (2007). Indoor ultrafine particles and childhood asthma: exploring a potential public health concern. *Indoor Air*, *17*, 81–91.
Wild, R.K. (1977). High temperature oxidation of austenitic stainless steel in low oxygen pressure. *Corrosion Science*, *17*(87–93), 95–104.
Yehia, A. and Mizuno, A., 2005. Silver discharge electrode for suppression of ozone generation in positive dc corona, In: Industry Applications Conference, 2005. Fourtieth IAS Annual Meeting. Conference Record of the 2005, A. Mizuno, ed., 1828–1832 Vol. 1823.
Yehia, A., mizuno, A., & takashima, K. (2000). On the characteristics of the corona discharge in a wire-duct reactor. *Journal of Physics D: Applied Physics*, *33*, 2807.
Zhuang, Y., Jin Kim, Y., Gyu Lee, T., & Biswas, P. (2000). Experimental and theoretical studies of ultra-fine particle behavior in electrostatic precipitators. *Journal of Electrostatics*, *48*, 245–260.